

Direct Confirmation of Two Pattern Speeds in the Double Barred Galaxy NGC 2950¹

E.M. Corsini², Victor P. Debattista³, and J.A.L. Aguerri⁴

ABSTRACT

We present surface photometry and stellar kinematics of NGC 2950, which is a nearby and undisturbed SB0 galaxy hosting two nested stellar bars. We use the Tremaine-Weinberg method to measure the pattern speed of the primary bar. This also permits us to establish directly and for the first time that the two nested bars are rotating with different pattern speeds, and in particular that the rotation frequency of the secondary bar is higher than that of the primary one.

Subject headings: galaxies: individual (NGC 2950) — galaxies: kinematics and dynamics — galaxies: elliptical and lenticular, cD — galaxies: photometry — galaxies: structure

1. Introduction

Large-scale bars are present in some 2/3 of all disk galaxies (Knapen et al 2000; Eskridge et al. 2000). Secondary stellar bars within large-scale bars are also common, occurring in about 1/3 of barred galaxies (Laine et al. 2002; Erwin & Sparke 2002). Interest in secondary stellar bars is motivated by the hypothesis that they are a mechanism for driving gas to small radii to feed the supermassive black holes powering active galactic nuclei (e.g. Regan & Mulchaey 1999). However, the efficiency of such transport is uncertain

¹Based on observations made with the UK Jacobus Kapteyn Telescope and Italian Telescopio Nazionale Galileo operated at the Spanish Observatorio del Roque de los Muchachos of the Instituto de Astrofísica de Canarias by Isaac Newton Group and Istituto Nazionale di Astrofisica, respectively.

²Dipartimento di Astronomia, Università di Padova, Vicolo dell'Osservatorio 2, I-35122 Padova, Italy, corsini@pd.astro.it

³Institut für Astronomie, ETH Hönggerberg, HPF G4.2, CH-8093 Zürich, Switzerland, debattis@phys.ethz.ch

⁴Instituto de Astrofísica de Canarias, Vía Láctea s/n, E-38200 La Laguna, Spain, jalfonso@ll.iac.es

because of the complete lack of knowledge of Ω_p and Ω_s , the pattern speeds of the primary and secondary bars. Whereas a number of pattern speeds of large-scale bars have been measured (see Aguerri et al. 2003, hereafter ADC03 and references therein), no such measurements in nested systems have been performed yet. The presence of nested bars with different pattern speeds has been inferred largely on the basis of their apparently random relative orientations (Buta & Crocker 1993). The possibility that $\Omega_s > \Omega_p$ is supported by the simulations of Rautiainen et al. (2002), which showed that secondary bars can naturally form and survive for more than few rotation periods in pure stellar disks. The morphological characteristics of these systems are suggestive of stars in the secondary bars oscillating about the loop orbits studied by Maciejewski & Sparke (2000) for models with $\Omega_s > \Omega_p$. However, simulations have also found other possibilities (Friedli & Martinet 1993), including cases where two stellar bars counter-rotate (Sellwood & Merritt 1994; Friedli 1996).

A model-independent method for measuring pattern speeds is the Tremaine-Weinberg method (Tremaine & Weinberg 1984, TW hereafter). This gives the pattern speed Ω of a single bar as

$$\mathcal{X}\Omega \sin i = \mathcal{V}, \quad (1)$$

where \mathcal{X} and \mathcal{V} are luminosity-weighted average position and line-of-sight velocity measured parallel to the major axis of the galaxy disk, and i is the disk inclination. Long-slit spectra parallel to the disk major-axis can measure all the quantities needed by Eqn. 1 provided that the galaxy is free of extinction. If several parallel slits at different offsets Y relative to the major axis are available for a galaxy, $\Omega \sin i$ can be obtained as the slope of a plot of \mathcal{V} versus \mathcal{X} . In a double barred galaxy (hereafter S2B), for a slit passing through both bars, Eqn. 1 is modified to

$$(\mathcal{X}_p\Omega_p + \mathcal{X}_s\Omega_s) \sin i = \mathcal{V} \quad (2)$$

provided the two bars are rigidly rotating through each other, i.e. that the total surface density is described by $\Sigma(R, \phi) = \Sigma_p(R, \phi - \Omega_p t) + \Sigma_s(R, \phi - \Omega_s t)$. Eqn. 2 is then a consequence of the linearity of the continuity equation. Eqn. 2 can be solved for Ω_s by first measuring Ω_p as in Eqn. 1 with slits which avoid the secondary bar, and then modeling to obtain \mathcal{X}_s from the observed $\mathcal{X} = \mathcal{X}_s + \mathcal{X}_p$. However, the two bars are not likely to rotate rigidly through each other when $\Omega_p \neq \Omega_s$ (Louis & Gerhard 1988; Maciejewski & Sparke 2000; Rautiainen et al. 2002), requiring additional modeling to obtain Ω_s . Nonetheless, when $\Omega_p = \Omega_s$, Eqn. 2 reduces to Eqn. 1 and is satisfied exactly. Thus testing whether $\Omega_s = \Omega_p$ does not require any assumptions.

2. NGC 2950

An ideal target for this purpose is the S2B NGC 2950, which is a large ($2'.7 \times 1'.8$ [de Vaucouleurs et al. 1991, hereafter RC3]) and bright ($B_T = 11.84$ [RC3]) early-type barred galaxy. NGC 2950 is classified RSB0(r) and its total absolute magnitude is $M_{B_T}^0 = -20.03$ (RC3) adopting a distance of 23.3 Mpc (Tully 1988). The presence of a secondary stellar bar has been discussed extensively by Wozniak et al. (1995), Friedli et al. (1996), and Erwin & Sparke (2002) on the basis of ground-based and *Hubble Space Telescope* images in both optical and near-infrared bandpasses. The secondary bar of NGC 2950 is typical of those in the samples of Laine et al. (2002) and of Erwin & Sparke (2002). NGC 2950 meets all the requirements for the TW analysis: it has an intermediate inclination, both bars have intermediate position angles (hereafter PA) between the major and minor axes of the disk and no evidence of spirals, patchy dust or significant companions.

3. Surface photometry

The photometric observations of NGC 2950 were carried out at the 1-m Jacobus Kapteyn Telescope on December 27-28, 2000. We took multiple exposures in the Harris B (4×1200 s), V (3×480 s), and I (18×150 s) bandpasses using the SITe2 2048×2048 CCD. This camera has a scale of $0''.33 \text{ pixel}^{-1}$, yielding an unvignetted field of view of $\sim 10' \times 10'$. The seeing FWHM was $\approx 1''.0$. The data reduction has been carried out using standard IRAF tasks as in Debattista et al. (2002, hereafter DCA02). Images were bias subtracted, flatfielded, cleaned of cosmic rays, and corrected of bad pixels. The sky-background level was removed by fitting a second-order polynomial to the regions free of sources. Photometric calibration, using standard stars, included corrections for atmospheric and Galactic extinction, and for color as in DCA02.

The radial profiles of surface brightness, ellipticity and PA were obtained by fitting elliptical isophotes with the IRAF task ELLIPSE. We first fitted ellipses allowing their centers to vary to test for patchy dust obscuration. We found no evidence of a varying center within the errors of the fits, and similar PA and ellipticity profiles for all bandpasses. Thus we concluded that there is little or uniform obscuration, as required for the TW method. The ellipse fits were then repeated with the ellipse center fixed; the resulting photometric profiles are plotted in Fig. 1. We interpreted the local maximum in ellipticity at $r \simeq 3''$ and the corresponding twist and stationary value in PA as the photometric signatures of the presence of a misaligned secondary bar inside the primary bar. This is confirmed by the analysis of $B - I$ and $V - I$ color maps and unsharp mask of the original frames; in all we find no evidence of other small-scale structures such as nuclear rings or disks, spiral

arms, star-forming regions, dust lanes and/or dust patches, in agreement with previous results (Wozniak et al. 1995; Friedli et al. 1996; Erwin & Sparke 2003). In particular, the structural details unveiled by the unsharp mask of the WFPC2/F814W image of the nucleus of NGC 2950 (Erwin & Sparke 2003) are unlike those typical of nuclear stellar disks (Pizzella et al. 2002). The PAs of the primary ($\text{PA}_p = 152^\circ 6 \pm 0^\circ 4$) and secondary bar ($\text{PA}_s = 91^\circ 1 \pm 0^\circ 3$) were measured in the I -band image at $r \simeq 3''$ and $r \simeq 23''$, at the two peaks in the ellipticity profile (Fig. 1). The lengths of the primary ($a_p = 34''.3 \pm 2''.1$) and secondary bar ($a_s = 4''.5 \pm 1''.0$) were measured using three independent methods based on Fourier amplitudes (Aguerri et al. 2000), Fourier and ellipse phases (DCA02), and a decomposition of the surface brightness profiles (Prieto et al. 2001). The inclination ($i = 45^\circ 6 \pm 1^\circ 0$) and PA of the disk ($\text{PA}_d = 116^\circ 1 \pm 1^\circ 0$) were determined by averaging the values measured between $65''$ and $100''$ in the I -band profile (Fig. 1).

4. Long-slit spectroscopy

The spectroscopic observations of NGC 2950 were carried out at the 3.6-m Telescopio Nazionale Galileo on December 18, 2001 (run 1), March 20-22, 2002 (run 2), and March 9-11, 2003 (run 3). The Low Resolution Spectrograph mounted the HR-V grism No. 6 with 600 grooves mm^{-1} and the $0''.7 \times 8''.1$ slit. The detector was the Loral CCD with 2048×2048 pixels of $15 \times 15 \mu\text{m}^2$. The wavelength range from 4660 to 6820 Å was covered with a reciprocal dispersion of $1.054 \text{ Å pixel}^{-1}$ and a spatial scale of $0.275 \text{ arcsec pixel}^{-1}$. We obtained 4 spectra with the slit along the disk major axis (run 2 and 3), and 11 offset spectra with the slit parallel to it ($Y = -3''.1, +1''.5, +2''.8, \pm 10''.1$ in run 1, $Y = \pm 5''.1, \pm 13''.4$ in run 2, and $Y = -2''.5, +3''.5$ in run 3, Fig. 2). The exposure times were $2 \times 60 \text{ min}$ and $2 \times 45 \text{ min}$ for the major-axis spectra obtained in run 2 and 3, respectively, and 45 min for all the offset spectra. Comparison lamp exposures before and/or after each object integration ensured accurate wavelength calibrations. Spectra of G and K giant stars served as kinematical templates. The seeing FWHM was $\approx 1''.2$ in run 1, $\approx 1''.5$ in run 2, and $\approx 0''.9$ in run 3. Using standard MIDAS routines, all the spectra were bias subtracted, flatfield corrected, cleaned of cosmic rays, corrected for bad pixels and wavelength calibrated as in DCA02. The accuracy of the wavelength rebinning ($\lesssim 2 \text{ km s}^{-1}$) was checked by measuring wavelengths of the brightest night-sky emission lines. The instrumental resolution was 3.10 Å (FWHM) corresponding to $\sigma_{inst} \approx 80 \text{ km s}^{-1}$ at 5170 Å. The major-axis spectra obtained in the same run were co-added using the center of the stellar continuum as reference. In all the spectra the contribution of the sky was determined by interpolating along the outermost $\approx 20''$ at the edges of the slit and then subtracted.

5. Pattern speeds of the primary bar and secondary bar

To measure \mathcal{V} for each slit (Fig. 3a), we first collapsed each two-dimensional spectrum along its spatial direction in the wavelength range between 5060 and 5490 Å, obtaining a one-dimensional spectrum. The value of \mathcal{V} was then derived by fitting the resulting spectrum with the convolution of the spectrum of the K1III star HR 4699 and a Gaussian line-of-sight velocity profile by means of the Fourier Correlation Quotient method (Bender 1990, hereafter FCQ) as done in ADC03. We estimated uncertainties by Monte Carlo simulations with photon, read-out and sky noise. To compute \mathcal{X} for each slit (Fig. 3b), we extracted the luminosity profiles from the V -band image along the position of the slit after convolving the image to the seeing of the spectrum. The V -band profiles match very well the profiles obtained by collapsing the spectra along the wavelength direction, confirming that the slits were placed as intended. We used the V -band profiles to compute \mathcal{X} because they are less noisy than those extracted from the spectra, particularly at large radii. We obtained Ω_p from the values of \mathcal{X} and \mathcal{V} for the slits at $|Y| \geq 3''.1$ and at $Y = 0''$ (the latter constrain only the zero point). Since the slits at $|Y| \geq 3''.1$ do not cross the secondary bar, we assume $\mathcal{X} = \mathcal{X}_p$ and $\mathcal{V} = \mathcal{V}_p$ for them and obtain $\Omega_p \sin i$ with a straight line fit. This gives $\Omega_p = 11.2 \pm 2.4 \text{ km s}^{-1} \text{ arcsec}^{-1}$ ($99.2 \pm 21.2 \text{ km s}^{-1} \text{ kpc}^{-1}$, Fig. 3c) The value of Ω_p does not change within errors ($\Omega_p = 10.9 \pm 2.4 \text{ km s}^{-1} \text{ arcsec}^{-1}$) when we exclude the slits at $Y = -3''.1, +3''.5$, confirming that they are not much affected by the secondary bar (Fig. 2).

We used the FCQ to measure the line-of-sight velocity and velocity dispersion profiles of the stellar component along the major axis (Fig. 4). All the major-axis spectra were co-added after being convolved to the same seeing. We derived the circular velocity in the disk region, $V_c = 356^{+61}_{-49} \text{ km s}^{-1}$, after a standard correction for the asymmetric drift as in ADC03. Thus the corotation radius of the primary bar is $D_p = V_c/\Omega_p = 32''.4^{+8.7}_{-6.2}$ and the ratio $\mathcal{R}_p \equiv D_p/a_p$ of the corotation radius to the bar semimajor axis is $\mathcal{R}_p = 1.0^{+0.3}_{-0.2}$ (error intervals on D_p and \mathcal{R}_p are 68% confidence level and were measured with Monte Carlo simulations as in ADC03). We conclude that, within the errors, the primary bar of NGC 2950 is consistent with all previous measurements of \mathcal{R} in SB0 galaxies (ADC03), which gives us confidence in our assumption that the signals in the outer slits are generated by the primary bar only.

The photometric and kinematic integrals measured with the innermost slits ($|Y| \leq 2''.8$) include a contribution from the secondary bar. In particular, $|\mathcal{V}| \gg |\mathcal{V}_p|$ for the slits at $Y = -2''.5, +2''.8$ if we extrapolate \mathcal{V}_p from large $|Y|$. A straight line fit to \mathcal{X} and \mathcal{V} for the slits at $|Y| \leq 2''.8$ has a slope ($= 63.7 \pm 7.1 \text{ km s}^{-1} \text{ arcsec}^{-1}$, Fig. 3c) which is different at better than 99% confidence level from the slope ($= 8.0 \pm 1.7 \text{ km s}^{-1} \text{ arcsec}^{-1}$, Fig. 3c)

of the straight line fit for the primary bar. This may be because $\Omega_p \neq \Omega_s$; however, to justify this conclusion, we needed to exclude the possibility of a systematic error due to PA errors, which \mathcal{X} and \mathcal{V} are quite sensitive to (Debattista 2003). We tested whether the difference in the slopes of the straight line fits may be due to only PA errors when $\Omega_p = \Omega_s$ by building a model of a S2B galaxy with a single pattern speed from an N -body simulation of a SB0 galaxy described in Debattista (2003). We rotated particles by 90° , rescaled their phase space coordinates by a factor of 0.2, and added them back to the original galaxy with various primary to secondary mass ratios to approximately match NGC 2950. After projecting this system as in NGC 2950, we proceeded to measure \mathcal{X} and \mathcal{V} for slits misaligned with the major axis. Even when PA errors reached $\pm 5^\circ$, we were not able to produce a system which approaches the behavior of our observations. In particular, we were not able to produce a system in which the slopes of the integrals plotted versus $|Y|$ are larger for \mathcal{V} and smaller for \mathcal{X} in the region of the secondary bar than in the region of the main bar, as we observed in NGC 2950 (Fig. 3a,b). We therefore concluded that the signatures we observed could not be an artifact of any PA misalignments on two bars rotating with a single pattern speed. Our results, therefore, lead us to conclude, directly and for the first time, that $\Omega_s \neq \Omega_p$.

However, estimating Ω_s is model dependent; we illustrate this by considering two extreme cases. First, we assumed that the secondary bar dominates at $|Y| \leq 2''.8$, and used Eqn. 1 with Ω replaced by Ω_s to find $\Omega_{s,1} = 89.2 \pm 9.9 \text{ km s}^{-1} \text{ arcsec}^{-1}$ (Fig. 3c). In the second case, we rewrote Eqn. 2 as $\mathcal{X}_s(\Omega_s - \Omega_p) \sin i = \mathcal{V} - \Omega_p \mathcal{X} \sin i$. The observed quantities are \mathcal{X} and \mathcal{V} , while Ω_p was measured above. To obtain \mathcal{X}_s , first we derived the values of \mathcal{X}_p in the region of the nuclear bar by fitting a straight line to the \mathcal{X} values at $|Y| \geq 10''.1$ (fits extending to smaller $|Y|$ give larger $|\Omega_s|$), and obtained $\mathcal{X}_s = \mathcal{X} - \mathcal{X}_p$. Then plotting $(\mathcal{V} - \Omega_p \mathcal{X} \sin i)$ versus \mathcal{X}_s , we obtain $(\Omega_s - \Omega_p) \sin i$ as the slope of the best fitting line; the result is $\Omega_{s,2} = -21.2 \pm 6.2 \text{ km s}^{-1} \text{ arcsec}^{-1}$, *i.e.* secondary bar counter-rotating relative to the primary. (Note that the range from $\Omega_{s,1}$ to $\Omega_{s,2}$ passes smoothly through $\pm\infty$, *i.e.* a vertical line.)

6. Conclusions

We showed that the primary bar in NGC 2950 is rapidly rotating. If this is the norm in S2B galaxies, then it guarantees that primary bars are efficient at funnelling gas down to the radius of influence of secondary bars. In Fig. 4, we plot the lines of slope $\Omega_{s,1} \sin i$ and $\Omega_{s,2} \sin i$. The range of Ω_s is large enough that it must include the case where $\mathcal{R}_s \simeq 1$. However, it also includes the case where $\mathcal{R}_s \sim 2$, which hydrodynamical simulations find

leads to inefficient gas transport (Maciejewski et al. 2002).

We suggest two avenues for fruitful future work. First, since the two bars cannot be in exact solid body rotation (Louis & Gerhard 1988; Maciejewski & Sparke 2000; Rautiainen et al. 2002), a more accurate measurement of Ω_s will require careful modeling and comparison with simulations to account for such effects. Second, it may be that secondary bars oscillate about an orientation perpendicular to the primary bar, possibly accounting for $\Omega_s < 0$. This can be tested by repeating our measurements on a sample of S2B galaxies. Nonetheless, we can confidently conclude that in NGC 2950 the two bars must have different pattern speeds, with the secondary bar having a larger pattern speed.

REFERENCES

- Aguerri J. A. L., Muñoz-Tuñón C., Varela A. M., & Prieto M. 2000, *A&A*, 361, 841.
- Aguerri, J. A. L., Debattista, V. P., & Corsini, E. M. 2003, *MNRAS*, 338, 465 (ADC03)
- Bender, R. 1990, *A&A*, 229, 441
- Buta, R., & Crocker, D. A., 2003, *AJ*, 105, 1344
- Debattista, V. P. 2003, *MNRAS*, 342, 1194
- Debattista, V. P., Corsini, E. M., & Aguerri, J. A. L. 2002, *MNRAS*, 332, 65 (DCA02)
- de Vaucouleurs, G., de Vaucouleurs, A., Corwin Jr., H. G., Buta, R. J., Paturel, G., & Fouqu , P. 1991, *Third Reference Catalogue of Bright Galaxies* (New York:Springer) (RC3)
- Erwin, P., & Sparke, L. S. 2002, *AJ*, 124, 65
- Erwin, P., & Sparke, L. S. 2003, *ApJS*, 146, 299
- Eskridge, P. B., et al. 2000, *AJ*, 119, 536
- Friedli, D. 1996, *A&A*, 312, 761
- Friedli, D., & Martinet, L. 1993, *A&A*, 277, 27
- Friedli, D., Wozniak, H., Rieke, M., Martinet, L., & Bratschi, P. 1996, *A&AS*, 118, 461
- Knapen, J. H., Shlosman, I., & Peletier, R. F. 2000, *ApJ*, 529, 93

- Laine, S., Shlosman, I., Knapen, J. H., & Peletier, R. F. 2002, *ApJ*, 567, 97
- Louis, P. D., & Gerhard, O. E. 1988, *MNRAS*, 233, 337
- Maciejewski, W., & Sparke, L. S. 2000, *A&A*, 313, 745
- Maciejewski, W., Teuben, P. J., Sparke, L. S., & Stone, J. M. 2002, *MNRAS*, 329, 502
- Pizzella, A., Corsini, E. M., Morelli, L., Sarzi, M., Scarlata, C., Stiavelli, M., & Bertola, F. 2002, *ApJ*, 573, 131
- Prieto, M., Aguerri, J. A. L., Varela, A. M., & Muñoz-Tuñón, C. 2001, *A&A*, 367, 405
- Rautiainen, P., Salo, H., & Laurikainen, E. 2002, *MNRAS*, 337, 1233
- Regan, M. W. & Mulchaey, J. S. 1999, *AJ*, 117, 2676
- Sellwood, J. A., & Merritt, D. 1994, *ApJ*, 425, 530
- Tremaine, S., & Weinberg, M. D. 1984, *ApJ*, 282, L5
- Tully, R. B. 1988, *Nearby Galaxy Catalog*, (Cambridge:CUP)
- Wozniak, H., Friedli, D., Martinet, L., Martin, P., & Bratschi, P. 1995, *A&AS*, 111, 115

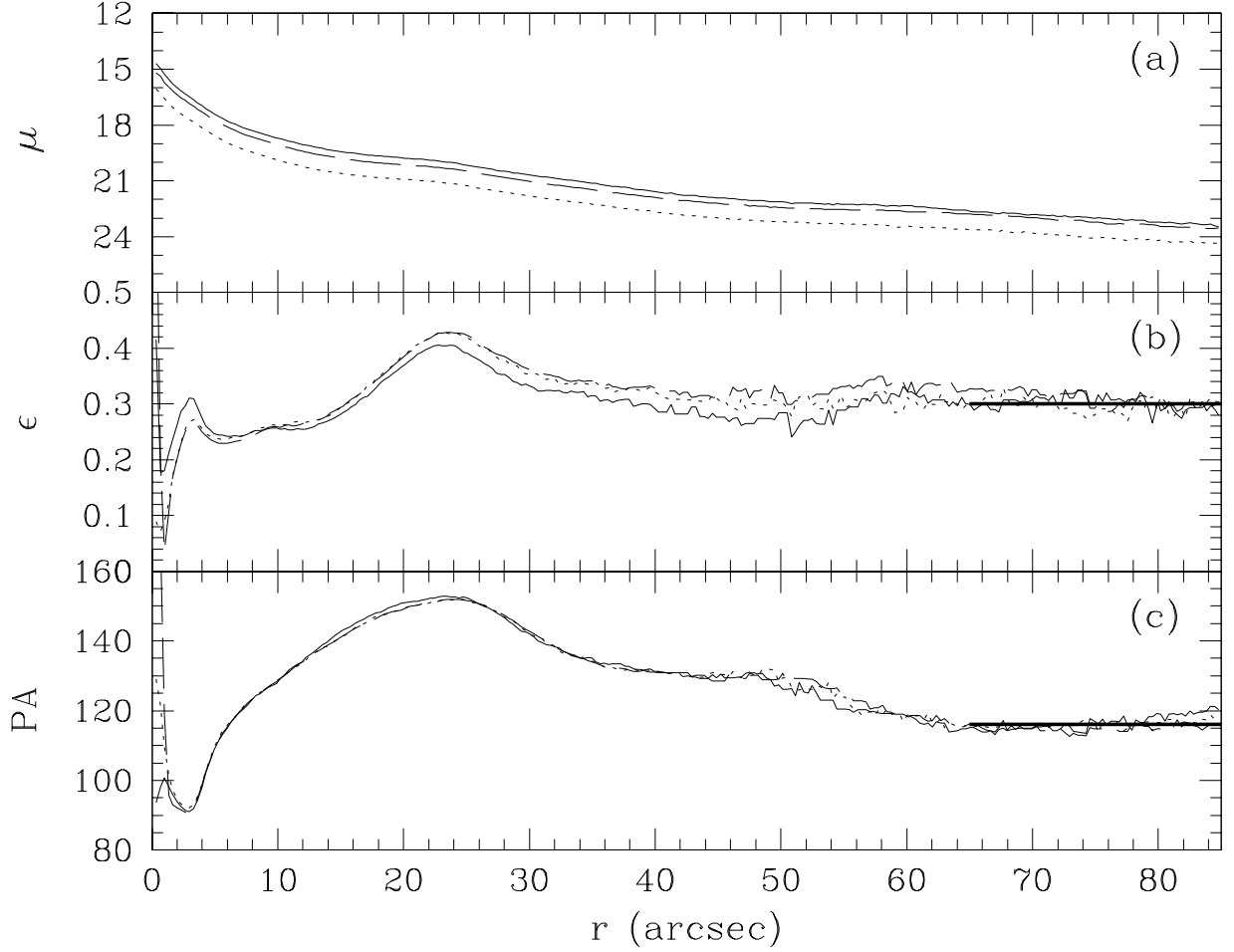


Fig. 1.— (a) Surface brightness, μ , (b) ellipticity, ϵ , and (c) PA radial profiles of NGC 2950. Solid, dashed and dotted lines refer to I , V , and B -band data, respectively. The thick lines represent the fits to the I -band ϵ and PA of the galaxy's disk.

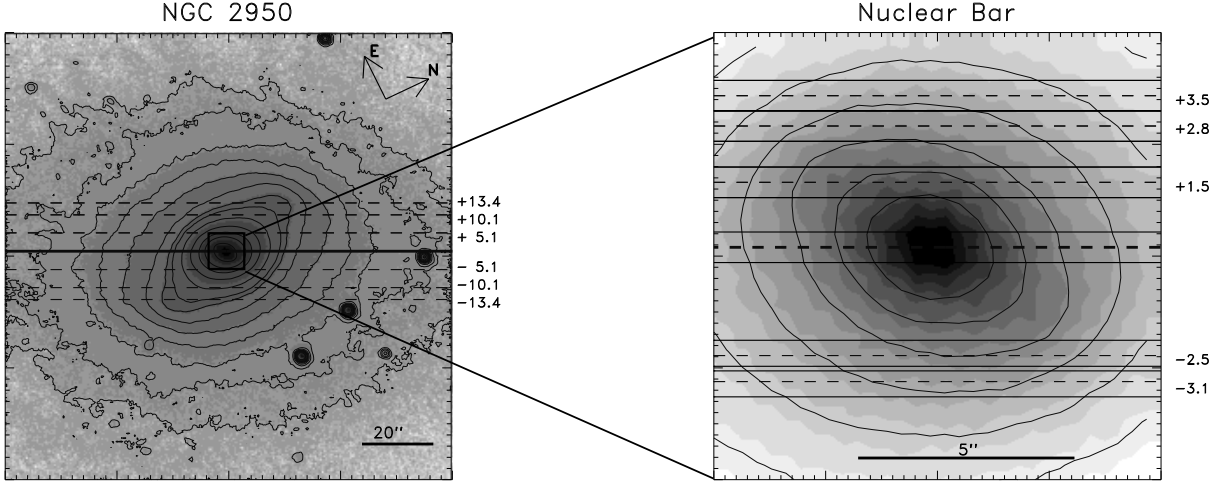


Fig. 2.— *Left panel:* Large-scale image of NGC 2950 showing the primary bar and disk with I -band contours and slit positions overlaid. Contours are spaced at $0.5 \text{ mag arcsec}^{-2}$ and the outermost corresponds to $\mu_I = 23.0 \text{ mag arcsec}^{-2}$. The solid and dashed lines correspond to the position of the spectra obtained along the disk major axis and at large offsets ($|Y| \geq 5''.1$), respectively. For each slit position the offset, Y , is given in arcsec (we arbitrarily chose axes such that Y increases from the SW to the NE sides). *Right panel:* A zoom into the central region of NGC 2950 showing its secondary bar. I -band isocontours are spaced at $0.5 \text{ mag arcsec}^{-2}$, with the outermost corresponding to $\mu_I = 19.5 \text{ mag arcsec}^{-2}$. For each spectrum obtained at $|Y| \leq 3''.5$ the solid and dashed lines mark the edges and center of the slit, respectively.

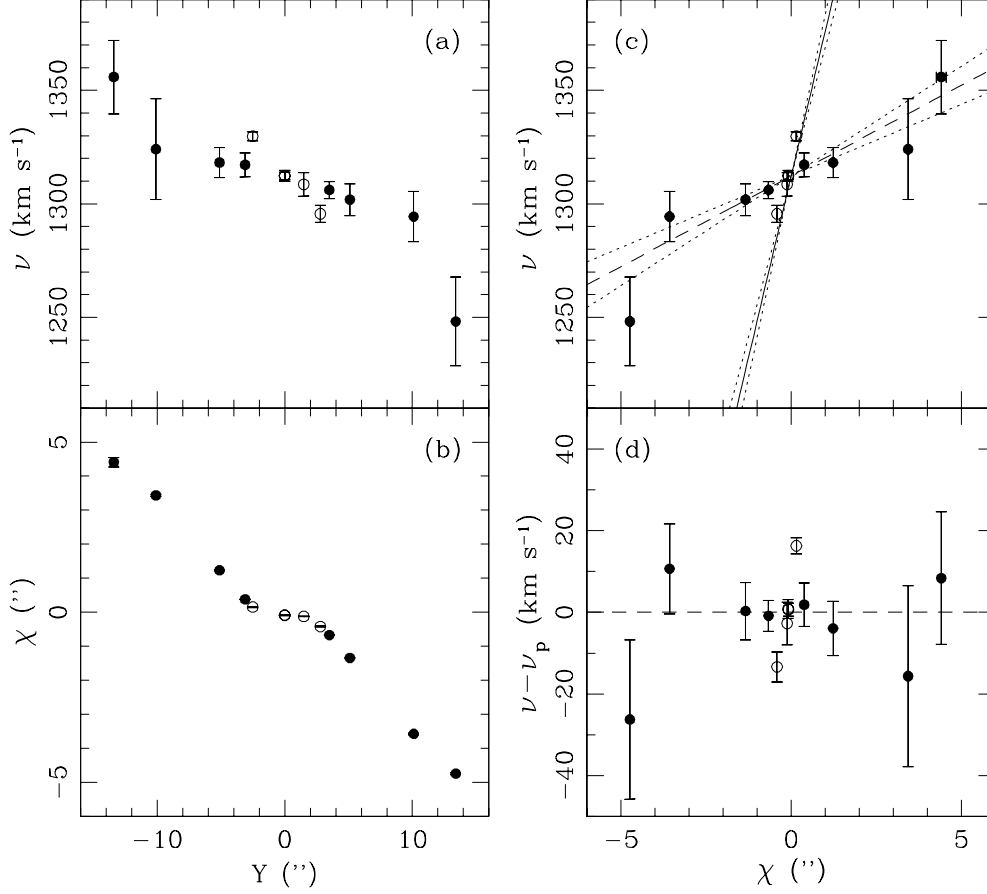


Fig. 3.— (a) The kinematic integrals \mathcal{V} as a function of the slit offset Y with respect to the major axis ($Y = 0''$). Open and filled circles correspond to slits crossing the secondary bar ($|Y| \leq 2''.8$) and only the primary bar ($|Y| \geq 3''.1$), respectively. (b) The photometric integrals \mathcal{X} as a function of the slit offset Y . (c) \mathcal{V} as a function of \mathcal{X} with different straight-line fits. These were obtained including the slits at $Y = 0''$ and only the slits at $|Y| \geq 3''.1$ (dashed line, slope $\Omega_p \sin i = 8.0 \pm 1.7 \text{ km s}^{-1} \text{ arcsec}^{-1}$) or the innermost slits at $|Y| \leq 2''.8$ (solid line, slope $\Omega_{s,1} \sin i = 63.7 \pm 7.1 \text{ km s}^{-1} \text{ arcsec}^{-1}$). The very different slopes of the two straight lines strongly suggest that the primary and secondary bars have different pattern speeds. (d) The residuals from the straight line fit to the slits at $|Y| \geq 3''.1$ and at $Y = 0''$.

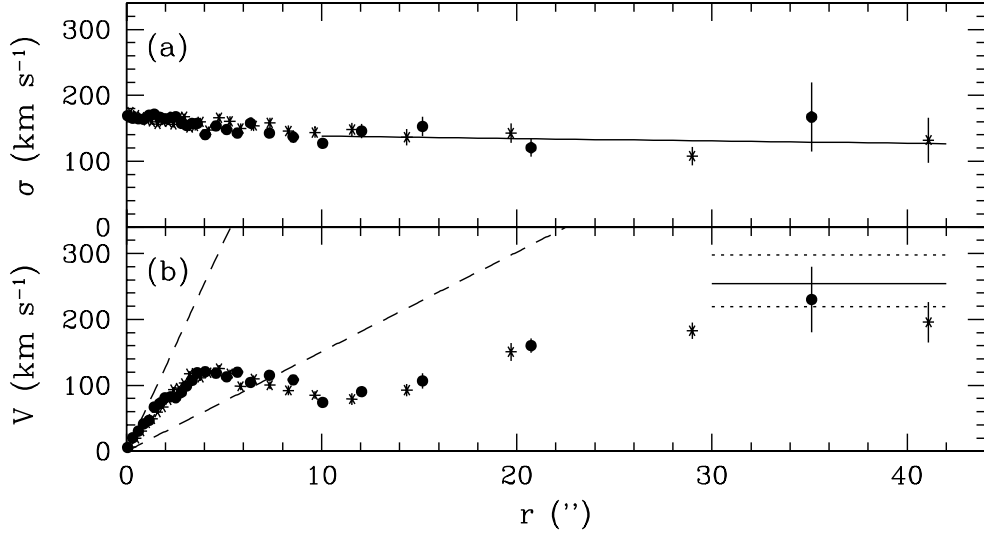


Fig. 4.— (a) The major-axis radial profile of the stellar line-of-sight velocity dispersion fitted with an exponential profile at $r \geq 10''$ (solid line). (b) The major-axis radial profile of the stellar line-of-sight velocity (after subtracting the systemic velocity $V_{sys} = 1312 \pm 3 \text{ km s}^{-1}$) and the $V_c \sin i$ curve (solid line) with errors (dotted lines) obtained by applying the asymmetric drift for $r \geq 30''$ as in ADC03. Dashed lines have slope $\Omega_{s,1} \sin i = 63.7 \text{ km s}^{-1} \text{ arcsec}^{-1}$ and $|\Omega_{s,2}| \sin i = 15.1 \text{ km s}^{-1} \text{ arcsec}^{-1}$. In (a) and (b) the measured profiles are folded around the center, with filled circles and asterisks referring to the SE (receding) and NW (approaching) sides, respectively.